Structure determination of heteroaromatic thiophene dimers by intermolecular Coulombic decay upon electron-impact ionization

Jiaqi Zhou,[1] Qingrui Zeng,[1] Chuncheng Wang,[2,*] Shaokui Jia,[1] Xiaorui Xue,[1] Xintai Hao,[1] Lanhai He,[2] Deepthy Maria Mootheril,[3] Alexander Dorn,[3] Dajun Ding,[2] and Xueguang Ren[1,†]

[1]*MOE Key Laboratory for Nonequilibrium Synthesis and Modulation of Condensed Matter, School of Physics, Xi'an Jiaotong University, Xi'an 710049, China*

[2]*Institute of Atomic and Molecular Physics, Jilin University, Changchun 130012, China*

[3]*Max-Planck-Institut für Kernphysik, Heidelberg 69117, Germany*

(Received 21 April 2024; accepted 26 July 2024; published 12 August 2024)

This paper reports the structure and intermolecular potential energy curve (PEC) of heteroaromatic thiophene dimers obtained using a cold-target recoil-ion momentum spectroscopy reaction microscope. The three-dimensional momenta and kinetic energy release (KER) of the $C_4H_4S^+ + C_4H_4S^+$ ion pairs are obtained by coincident momentum measurement. The two-body dissociation channel is initiated either by the rapid removal of one outer-valence electron from each thiophene molecule via sequential ionization or by intermolecular Coulombic decay (ICD). Our analysis of the absolute cross sections indicates that the $C_4H_4S^+ + C_4H_4S^+$ ion pair is preferentially formed by the ICD process. The measured KER and PEC, accompanied by *ab initio* molecular dynamics simulations for three different types of conformers, enable us to clarify the minimum energy configuration of thiophene dimers in the gas phase. These results are helpful for our understanding of π-π and σ-π interactions within heteroaromatic ring complexes.

DOI: 10.1103/PhysRevA.110.022809

I. INTRODUCTION

The heteroaromatic moiety thiophene plays a crucial role in accurately understanding noncovalent interactions between molecular species, which is essential for a variety of fundamental scientific inquiries and applications, such as the development of conductors [1,2], electrode materials [3,4], and organic semiconductors [5,6]. The characteristic polyconjugated nature of the thiophene polymer allows the intermolecular delocalization of π electrons resulting in the reduction of the band gap [7], which determines its electronic and nonlinear optical properties [8,9]. Knowledge of the structural preference of thiophene dimers dictates how the units are bonded by van der Waals forces and sheds light on the factors influencing electronic overlap, such as the orientation and distance between adjacent molecules.

Investigations on molecular complexes with a small number of moieties are essential to understand how changes in noncovalent interactions influence structural arrangements. Several theoretical and experimental studies investigated the correlation between the structure and stability of small aromatic complexes [10–21]. In the case of a conjugated thiophene dimer, the calculations showed that it can be placed either in a stacking, T-shaped, or coplanar arrangement [14–17]. The stacking and T-shaped configurations were found to be stable, while planar configurations lie higher in energy. Nevertheless, due to the similar interaction energies of stacking and T-shaped structures [14–16,21], and the strong basis set dependence of *ab initio* calculations, the more stable one among them is still a subject of debate.

Gas-phase data are particularly helpful for clarifying this controversy, as experimental results can be directly compared with theory. In this paper, we study the structural properties of thiophene dimers by double ionization and subsequent Coulomb explosion, which has been proven to be a feasible method for reconstructing intermolecular distances in clusters [22–31]. Coincidence momentum imaging provides kinematically complete information on the Coulomb explosion process, where the three-dimensional momentum vectors of all product ions resulting from a single parent ion are determined. This dynamical information is closely related to the positions of charges and nuclei prior to the dissociation in the molecular frame, which enables us to deduce the initial configuration of the molecular systems. It is worth noting that the nuclei must be "frozen" during the double ionization process before the Coulomb explosion to prevent structural deformation, which requires an ultrafast ionization reaction.

One effective method of achieving ultrafast ionization is electron collision, where the outer-valence electrons of molecular clusters can be quickly ionized by two different mechanisms. One involves the sequential ionization (SI) of an outer valence electron from each molecule. The other pathway involves inner-valence ionization, followed by ultrafast radiationless energy transfer from the excited species to its neighbor. The energy transferred leads to the emission of one electron from the neutral neighbor, which is known as intermolecular Coulombic decay (ICD) [32]. Both ionization processes proceed on the femtosecond timescale [29,33,34],

*Contact author: ccwang@jlu.edu.cn
†Contact author: renxueguang@xjtu.edu.cn

during which the slower motion of the molecular complexes relative to each other can be neglected.

Here, we clarified the minimum energy configuration of the neutral thiophene dimer ($^1A'$) through a Coulomb explosion induced by electron-impact ionization (200 eV). Two product ions ($C_4H_4S^+$) are detected in coincidence, and six momentum vector components (three for each fragment ion) are determined for a single explosion event. The measured kinetic energy release (KER) of the Coulomb explosion channel is compared with the *ab initio* calculations of three different conformers of thiophene dimers. The consistency between the calculated results of different initial configurations and measured KER reveals the most stable structure of the gas-phase thiophene dimer, and the result is further supported by the potential energy curve (PEC) of the thiophene dimer deduced from the measured KER spectrum.

II. EXPERIMENTAL METHODS

The experiment was performed using a cold-target recoil-ion momentum spectrometer (COLTRIMS) located at the Xi'an Jiaotong University. The details of the experimental setup have been introduced elsewhere [35–37], and here we provide only a brief overview. The thiophene dimers are generated through a supersonic gas expansion of thiophene and the carrier gas helium at room temperature. The neutral molecular dimers are ionized by a well-focused pulsed electron beam (40 kHz) that is emitted from an electron gun, in which the tantalum photocathode is irradiated by a pulsed ultraviolet laser beam (0.5 ns pulse duration). The cations produced in the electron-molecule interaction are extracted by a uniform electric field (25 V/cm) onto a temporal and position-sensitive detector. During off-line analysis, the three-dimensional momentum vector of each detected cation is reconstructed from the measured time of flight (TOF) and position. Additionally, the momentum conservation condition is applied to filter out false coincidences.

III. THEORETICAL MODELS

We simulated the intermolecular and intramolecular dynamics during the Coulomb explosion of the doubly ionized dimer in order to quantify the partitioning of the Coulomb potential energy into center-of-mass kinetic energy and internal rovibrational energy. As starting point the neutral dimer geometry was taken and the time propagation was conducted over 500 fs. These *ab initio* molecular dynamics (AIMD) simulations were performed using the GAUSSIAN 16 package [38]. We consider three different types of conformers of thiophene dimers: parallel displaced (PD), T-shaped (T), and coplanar (C) conformers. As shown in Fig. 1, the planes of two thiophene molecules have either a parallel or perpendicular orientation to each other. The initial conditions, i.e., geometries of a neutral dimer, were sampled by the quasiclassical fixed normal-mode sampling method under the temperature of the gas target (30 K). The populations of the initial vibrational states of the thiophene dimer were determined by Boltzmann distributions. The molecular dynamics simulations were performed under the extended Lagrangian molecular dynamics scheme, adopting the so-called atom-centered density matrix

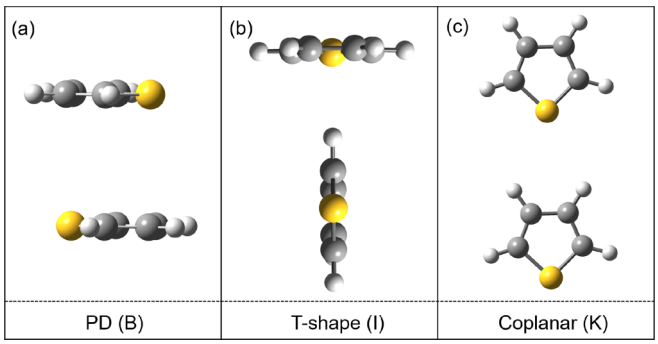

FIG. 1. Schematic of geometries of the thiophene dimers. (a) Parallel displaced, (b) T-shaped, and (c) coplanar configurations. All structures are selected from Ref. [15] (*B*, *I*, *K*), which are optimized at the MP2/6-311G** level.

propagation (ADMP) method [39–41] using the density-functional theory (DFT) method at the Becke three-parameter Lee-Yang-Parr/correlation-consistent polarized valence double zeta (B3LYP/cc-pVDZ) functional level. All atoms were characterized by their three-dimensional momentum vectors. Propagation was performed for a duration of 500 fs with a time step of 0.5 fs. The total KER can be calculated by adding the kinetic energies of the simulated molecular ions together with the remaining Coulomb potential energy considering the center-of-mass distance at $t = 500$ fs [42,43].

IV. RESULTS AND DISCUSSION

In the experiment, the thiophene dimers can be ionized by two ultrafast ionization mechanisms, i.e., SI and ICD. As illustrated in Fig. 2, for the SI, the incident electron sequentially knocks out an outer-valence ($1a_2$) electron from each thiophene molecule. The electron scattering process occurs on a subfemtosecond timescale for a 200 eV impinging electron, which is much faster than the timescale of nuclear movement.

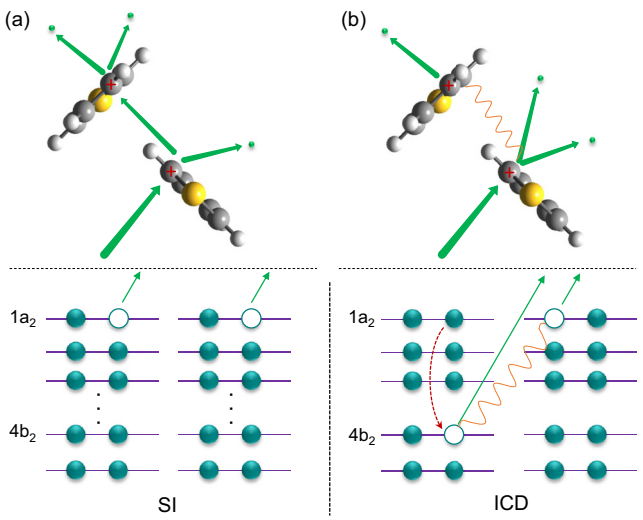

FIG. 2. Schematic of (a) SI and (b) ICD. The green and red arrows denote electron emission and intramolecular deexcitation, respectively. The orange wavy line denotes intermolecular energy transfer.

The SI has a threshold of about 20.88 eV, which is estimated by adding up the single ionization potentials of two thiophene molecules (9.0 eV × 2) [44] and the Coulomb energy (about 2.88 eV) at an intermolecular distance of 5.0 Å (the intermolecular distance of the T-shaped configuration). The ICD process occurs on the femtosecond timescale [33,34,45], which is also much faster than the intermolecular motion. The intermolecular vibrational period of the thiophene dimer is greater than 1 ps [46], which is much longer than the ICD lifetime (∼100 fs) [33,34,45]. Therefore, the structural changes in the dimer due to intermolecular vibrations during the double ionization process are negligible. In the thiophene dimer, the ICD process can be initiated by ionizing one inner-valence electron ($4b_2$) [44] with the binding energy above the dimer double ionization threshold. The outer-valence electron transitions downward to fill the inner-valence hole, releasing excess energy resulting in the ionization of the neighboring thiophene molecule. The contribution of SI and ICD can be estimated by calculating the absolute cross sections of the two processes. The absolute cross section of SI is estimated as the product of the cross sections of two sequential ionization steps [47,48], which is expressed as

$$\sigma_{\mathrm{SI}}(E_0) = \sigma^{+}_{C_4H_4S}(E_0)\frac{\sigma^{+}_{C_4H_4S}(E_1)}{4\pi R^2}. \quad (1)$$

The first term refers to the partial ionization cross sections for the first collision partner, and the latter is the possibility to ionize subsequently the other thiophene molecule. Here, $\sigma^{+}_{C_4H_4S}(E_0) \approx \sigma^{+}_{C_4H_4S}(E_1) \approx 2.78 \times 10^{-16}$ cm^2, which is determined by the ionization cross sections for electron collision with thiophene [49] and the proportion of $C_4H_4S^+$ parent ions in the mass spectrum [50]. $R = 5.0$ Å is the intermolecular distance for the T-shaped configuration of the thiophene dimers [15]. As a result, the cross section of SI is determined as 2.46×10^{-18} cm^2. If the ICD decay channel is open it is normally faster than other decay modes such as internal conversion which dominates the decay of inner-valence vacancies in monomers. Since the influence of neighboring molecules on the inner-valence ionization cross sections of thiophene is minor, the inner-valence ionization cross sections of thiophene dimers and monomers are nearly identical [31]. The cross section of the ICD process can be estimated as the cross section of the inner-valence ionization of the thiophene molecule. The inner-valence ionization of thiophene monomer leads to the C_3H^+ and C_4H^+ fragments [51], whose cross sections (i.e., cross sections of the ICD process) are 2.55×10^{-17} cm^2. Therefore, the analysis of the calculated absolute cross sections indicate that the contribution of ICD (2.55×10^{-17} cm^2) is dominant in comparison with SI (2.46×10^{-18} cm^2) in the double ionization of thiophene dimers. This result is consistent with the previous studies on ICD, where the cross section for SI was estimated to be approximately 20% in comparison with the ICD cross section [30,48,52]. Electron and ion coincidence experiments could give more insight and possibly clarify the contributions of SI and ICD [11,29].

Upon direct ionizing of two electrons at the equilibrium dimer configuration, the initially bound thiophene dimers transition to the Coulomb repulsion state followed by dissociation. The generated ion fragments are measured in coincidence, and their mass-to-charge ratios and three-dimensional momentum vectors are determined. The $C_4H_4S^+ + C_4H_4S^+$ channel is identified in the time-of-flight correlation spectrum of two measured cations. As shown in Fig. 3, the fragmentation channel displays a sharp diagonal structure with a slope of −1, due to the back-to-back emission of two cations and the momentum conservation. The dispersed background is attributed to the dissociation of larger clusters, wherein at least one neutral thiophene is emitted [11]. The recoil momenta due to the undetected neutral species result in the broadening of the correlation line. The vertical and horizontal lines originate from false coincidences. The distributions at the dashed and dotted lines are attributed to the ^{13}C and ^{34}S isotope channels.

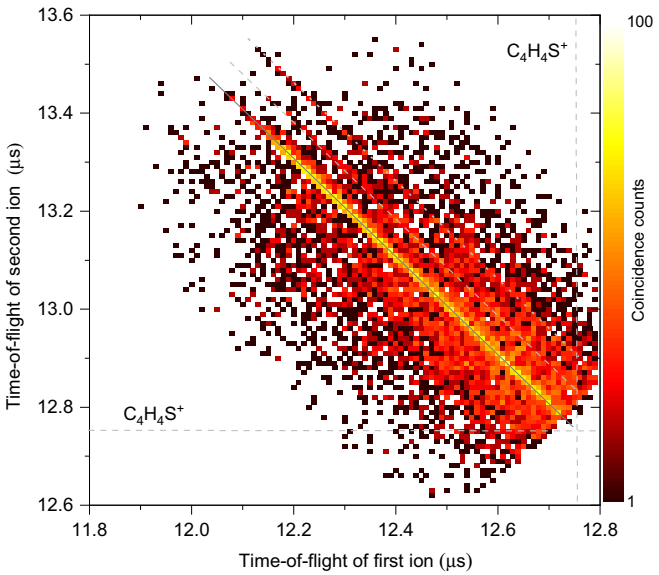

FIG. 3. Experimental TOF correlation spectrum of two measured cations. The distributions at the solid, dashed, and dotted diagonal lines show the $C_4H_4S^+ + C_4H_4S^+$ two-body dissociation channel, and the ^{13}C and ^{34}S isotope channels, $C_4H_4S^+ + ^{13}CC_3H_4S^+$ and $C_4H_4S^+ + C_4H_4^{34}S^+$, respectively. The color bar is linear which represents the number of measured coincidence counts.

The measured kinetic energy release (KER) spectrum of the $C_4H_4S^+ + C_4H_4S^+$ is presented in Fig. 4, which exhibits a dominant peak at approximately 2.6 eV with two shoulders at around 1.9 and 3.3 eV, respectively. The KER of the Coulomb explosion channel depends sensitively on the initial intermolecular distance and the orientation of the thiophene dimer, thereby providing important information about the initial configuration of molecular dimers. The intermolecular center-of-mass distances of the three configurations are quite different, and they are about 4.0, 5.0, and 6.4 Å for the parallel displaced, T-shaped, and coplanar conformers, respectively. This allows us to reconstruct the minimum energy configuration of the thiophene dimer. When we neglect the internal energy conversion during the Coulomb explosion, the intermolecular distance restored by the KER (2.6 eV) is about 5.5 Å. This coarse estimation is inconsistent with the intermolecular distance of all three structures (4.0, 5.0, and 6.4 Å).

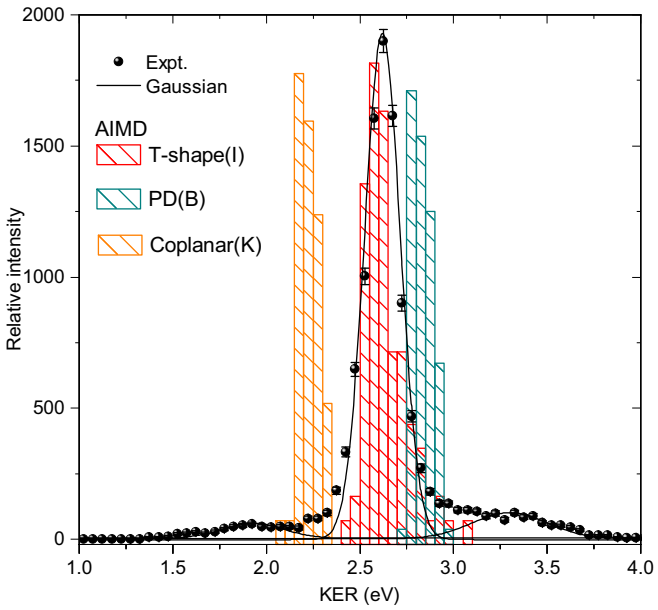

FIG. 4. The experimental and calculated KER of the $C_4H_4S^+ + C_4H_4S^+$ two-body dissociation channel. The black dots correspond to the experimental KER with multipeak Gaussian fitting results, and the orange, red, and green bars are the simulated KER for coplanar, T-shaped, and PD conformers, respectively.

An accurate method for elucidating the correlation between KER and molecular configuration is an *ab initio* molecular dynamics simulation. First, the structures of three different thiophene dimer conformers are optimized using the second-order Møller-Plesset perturbation theory (MP2) method and the 6-311G** basis set. The dimerization of the thiophene molecules is mainly driven by long-range interactions such as electrostatic and dispersion forces [15,16]. Here, we determined the configurations of three conformers from Ref. [15], where the geometries were optimized at the MP2/6-311G** level and the correction of the basis set superposition error (BBSE) is considered.

Second, the AIMD simulations are initiated by sampling the optimized thiophene dimer at a finite temperature (30 K) and stripping the two outermost electrons from the complex. Here, we have neglected the deformation of the molecular structure during the ionization process assuming instantaneous SI or ICD. In the simulations, all trajectories terminated as $C_4H_4S^+ + C_4H_4S^+$ and the KER of each trajectory is calculated as the sum of the kinetic energies of the cationic fragments at a propagation time of $t = 500$ fs and the remaining Coulomb potential at the intermolecular distance R ($t = 500$ fs) ranging from 8.48 to 16.74 Å.

The simulated KER distributions from the three conformers have been integrated into Fig. 4 and compared with the experimental results. All of them exhibit a single-peak structure with peaks located at 2.2, 2.6, and 2.8 eV for coplanar, T-shaped, and PD configurations, respectively. Among these configurations, the simulated KER distribution from the T-shaped structure agrees very well with the main peak, indicating that the T-shaped dimer is the dominant structure of the thiophene dimers in the gas jet. The contributions of coplanar and PD configurations are minor, and these cause the two shoulders. This result is consistent with the previous calculations, where the intermolecular interaction energies for the coplanar, T-shaped, and PD isomers are −31.7, −135.2, and −74.1 meV, respectively [18]. This indicates that the T-shaped structure is the most stable, followed by the PD and coplanar conformers. Additionally, by analyzing the measured KER using a multipeak fitting, we determined the branching ratios for the coplanar, T-shaped, and PD isomers to be roughly 0.04 : 0.86 : 0.10. The difference of measured and simulated KER distributions of coplanar and PD configurations may originate from the accuracy of the calculation methods, and the contributions of other coplanar (*L*-*Q* in Ref. [18]) and parallel (*A*, *C* in Ref. [18]) structures. Thus, the T-shaped configuration is designated as the more stable one. It is noted that the KER of the Coulomb explosion derived from the T-shaped configuration is about 0.28 eV smaller than the Coulomb potential at the equilibrium structure, which indicates the portion of the Coulomb repulsion energy which is converted into the internal energy of the cationic fragments, e.g., rotational and vibrational energy [42,43]. The accuracy of the computational methods and contributions from excited states could also contribute to the differences between the experimental results and theoretical calculations.

Based on the relation between the KER and intermolecular center-of-mass distance, we can reconstruct the shape of the intermolecular PEC of the thiophene dimer using the measured KER spectrum. For a bound dimer system, the Schrödinger equation is typically considered as the condition equation for the wave function $\Psi(R)$ of the system, which determines the full functional dependence of the interaction potential $V(R)$ between the particles [53],

$$V(R) = \frac{\frac{\hbar^2}{2\mu}\frac{d^2\Psi(R)}{dR^2}}{\Psi(R)} + E. \tag{2}$$

The wave function of the vibrational ground state of the dimer is real valued and positive. Therefore, such wave functions are experimentally accessible by determining their density distribution [53,54]. Here, the KER distribution is determined by the square of the ground-state wave function, $|\Psi(R)|^2$ [as shown in Fig. 5(a)]. R is the intermolecular distance and E is the binding energy of the dimer. R is deduced from the Coulomb repulsion potential with a further correction considering the conversion of Coulomb potential energy into the vibrational as well as rotational energy,

$$R = \frac{kq_1q_2}{\mathcal{R}_{\mathrm{KER}}} - 0.53\ \text{Å}. \tag{3}$$

k is the electrostatic constant. Here, 0.53 Å is an approximate correction value considering the R (5.53 Å) restored for T-shaped structures and the actual R (5.0 Å). By measuring a significant number of Coulomb explosion events, we can derive the distribution of the nuclear distances R that occur within the system. This distribution, in turn, directly corresponds to the measurement of the square of the vibrational wave function. $d^2\Psi(R)/dR^2$ is computed numerically by analyzing the second derivative of the $\Psi(R)$. To reduce the statistical fluctuations, the curvature was calculated encompassing five adjacent data points instead of three.

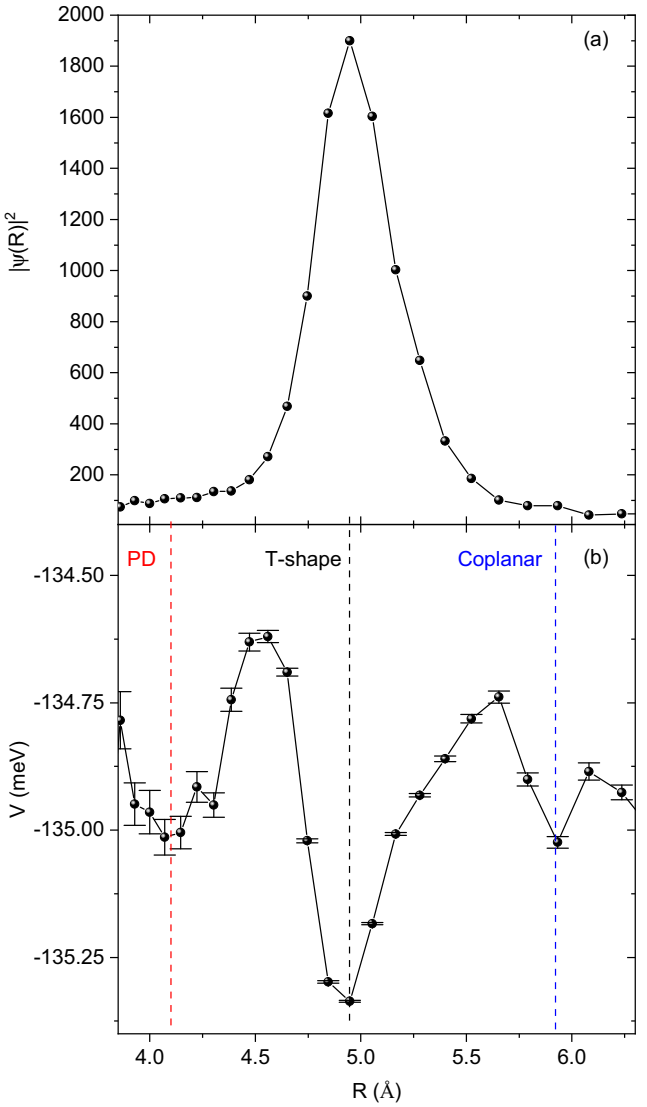

FIG. 5. (a) $|\Psi(R)|^2$ and (b) intermolecular potential energy curve of thiophene dimers obtained from the measured KER. The red, black, and blue dashed lines indicate three minima, which correspond to the PD, T-shaped, and coplanar conformers, respectively.

The result of $V(R)$ obtained from the measured KER distribution and using Eqs. (2) and (3) is shown in Fig. 5. For the energy scale an offset of 135 meV was chosen which is the binding energy of the dominant T-shaped conformer [15]. There are three minima on the PEC located at $R \sim 4.1$, 4.9, and 5.9 Å, respectively. The positions of three minima enable us to identify the different conformers. The global minimum on the PEC corresponds to the bound T-shaped conformers, while the other local minima belong to the bound PD and coplanar configurations. Furthermore, the T-shaped configuration has a higher binding energy than the PD structure, which confirms that the T-shaped configuration is more stable than the PD conformer in the gas phase. Unlike atoms, the center of mass and the center of charge in molecules may not coincide, which could lead to errors in the aforementioned calculations, but it can still reveal qualitatively the characteristics of the dimer PECs [54].

V. CONCLUSIONS

In conclusion, we have investigated the minimum energy configurations of thiophene dimers by multiparticle coincidence momentum spectroscopy combined with *ab initio* molecular dynamics simulations. The KER of the two-body fragmentation channel $C_4H_4S^+ + C_4H_4S^+$ is determined by the coincident momentum measurement of fragmentation ions. The $C_4H_4S^+$-$C_4H_4S^+$ intermediate dication is primarily accessed through ICD, which has a higher cross section compared to the SI process. The ICD occurs on an ultrafast femtosecond timescale such that nuclear motion can be neglected. The fragmentation dynamics of the $C_4H_4S^+$-$C_4H_4S^+$ dication are interpreted with the help of AIMD simulations. We calculated the KER of three different types of configurations, PD, T-shaped, and coplanar conformers, among which the simulated KER of the T-shaped structure responds well to the experimental spectrum indicating the dominant contribution of T-shaped thiophene dimers in the supersonic gas jet, while the populations of PD and coplanar configurations are minor. Furthermore, the sum of the PECs of the thiophene dimers is obtained using the measured KER, which indicates that the T-shaped conformer is more stable than the PD and coplanar structures. Current research on π-stacking interactions shows that the stability of heterocyclic dimers depends on the orientation between molecules. Despite the electrostatic interaction being weaker than the dispersion interaction, it is highly orientation dependent. This indicates that electrostatic interactions play an important role in the intermolecular interaction of heterocyclic dimers. These results are expected to be applicable to the reconstruction of PEC and configuration for molecular complexes, and to expand our understanding of the π-π and σ-π interactions between aromatic rings. Furthermore, the current findings can distinguish molecular complex isomers that are challenging for theoretical calculations, and can also serve as a powerful tool for comprehensively testing theoretical models.

ACKNOWLEDGMENTS

This work was jointly supported by the National Natural Science Foundation of China under Grants No. 12325406, No. 92261201, and No. 11974272, and Shaanxi Fundamental Science Research Project for Mathematics and Physics under Grant No. 22JSY022.

[1] T. Nezakati, A. Seifalian, A. Tan, and A. M. Seifalian, Conductive polymers: Opportunities and challenges in biomedical applications, Chem. Rev. **118**, 6766 (2018).

[2] K. Ueda, R. Fukuzaki, T. Ito, N. Toyama, M. Muraoka, T. Terao, K. Manabe, T. Hirai, C.-J. Wu, S.-C. Chuang, S. Kawano, and M. Murata, A highly conductive n-type coordination complex

with thieno[3,2-*b*]thiophene units: Facile synthesis, orientation, and thermoelectric properties, J. Am. Chem. Soc. **144**, 18744 (2022).

[3] C. E. Smith, S. O. Odoh, S. Ghosh, L. Gagliardi, C. J. Cramer, and C. D. Frisbie, Length-dependent nanotransport and charge hopping bottlenecks in long thiophene-containing π-conjugated molecular wires, J. Am. Chem. Soc. **137**, 15732 (2015).

[4] Y. Ie, K. Tanaka, A. Tashiro, S. K. Lee, H. R. Testai, R. Yamada, H. Tada, and Y. Aso, Thiophene-based tripodal anchor units for hole transport in single-molecule junctions with gold electrodes, J. Phys. Chem. Lett. **6**, 3754 (2015).

[5] N. Keller, D. Bessinger, S. Reuter, M. Calik, L. Ascherl, F. C. Hanusch, F. Auras, and T. Bein, Oligothiophene-bridged conjugated covalent organic frameworks, J. Am. Chem. Soc. **139**, 8194 (2017).

[6] T. Matsui, Y. Imamura, I. Osaka, K. Takimiya, and T. Nakajima, Analyses of thiophene-based donor–acceptor semiconducting polymers toward designing optical and conductive properties: A theoretical perspective, J. Phys. Chem. C **120**, 8305 (2016).

[7] M. Tachibana, S. Tanaka, Y. Yamashita, and K. Yoshizawa, Small band-gap polymers involving tricyclic nonclassical thiophene as a building block, J. Phys. Chem. B **106**, 3549 (2002).

[8] A. M. Valencia and C. Cocchi, Electronic and optical properties of oligothiophene-F4TCNQ charge-transfer complexes: The role of the donor conjugation length, J. Phys. Chem. C **123**, 9617 (2019).

[9] T. Zheng, Z. Cai, R. Ho-Wu, S. H. Yau, V. Shaparov, T. Goodson III, and L. Yu, Synthesis of ladder-type thienoacenes and their electronic and optical properties, J. Am. Chem. Soc. **138**, 868 (2016).

[10] M. Schnell, U. Erlekam, P. Bunker, G. von Helden, J.-U. Grabow, G. Meijer, and A. Van Der Avoird, Structure of the benzene dimer—governed by dynamics, Angew. Chem., Int. Ed. **52**, 5180 (2013).

[11] X. Ren, J. Zhou, E. Wang, T. Yang, Z. Xu, N. Sisourat, T. Pfeifer, and A. Dorn, Ultrafast energy transfer between π-stacked aromatic rings upon inner-valence ionization, Nat. Chem. **14**, 232 (2022).

[12] D. B. Ninković, J. M. Andrić, and S. D. Zarić, Parallel interactions at large horizontal displacement in pyridine–pyridine and benzene–pyridine dimers, ChemPhysChem **14**, 237 (2013).

[13] S. Kumar, P. Biswas, I. Kaul, and A. Das, Competition between hydrogen bonding and dispersion interactions in the indole $\cdots$ pyridine dimer and $(\text{Indole})_2 \cdots$ pyridine trimer studied in a supersonic jet, J. Phys. Chem. A **115**, 7461 (2011).

[14] A. Malloum and J. Conradie, Non-covalent interactions in small thiophene clusters, J. Mol. Liq. **347**, 118301 (2022).

[15] S. Tsuzuki, K. Honda, and R. Azumi, Model chemistry calculations of thiophene dimer interactions: origin of π-stacking, J. Am. Chem. Soc. **124**, 12200 (2002).

[16] I. D. Mackie, S. A. McClure, and G. A. DiLabio, Binding in thiophene and benzothiophene dimers investigated by density functional theory with dispersion-correcting potentials, J. Phys. Chem. A **113**, 5476 (2009).

[17] D. Kokkin, M. V. Ivanov, J. Loman, J.-Z. Cai, R. Rathore, and S. A. Reid, Strength of π-stacking, from neutral to cation: Precision measurement of binding energies in an isolated π-stacked dimer, J. Phys. Chem. Lett. **9**, 2058 (2018).

[18] S. Tsuzuki, K. Honda, T. Uchimaru, and M. Mikami, High-level *ab initio* computations of structures and interaction energies of naphthalene dimers: Origin of attraction and its directionality, J. Chem. Phys. **120**, 647 (2004).

[19] B. K. Mishra, J. S. Arey, and N. Sathyamurthy, Stacking and spreading interaction in N-heteroaromatic systems, J. Phys. Chem. A **114**, 9606 (2010).

[20] S. Tsuzuki, T. Uchimaru, A. Wakisaka, and T. Ono, Magnitude and directionality of halogen bond of benzene with C_6F_5X, C_6H_5X, and CF_3X (X = I, Br, Cl, and F), J. Phys. Chem. A **120**, 7020 (2016).

[21] M. Jacobs, L. Greff Da Silveira, G. Prampolini, P. R. Livotto, and I. Cacelli, Interaction energy landscapes of aromatic heterocycles through a reliable yet affordable computational approach, J. Chem. Theory Comput. **14**, 543 (2018).

[22] X. Xie, C. Wu, Y. Liu, W. Huang, Y. Deng, Y. Liu, Q. Gong, and C. Wu, Identifying isomers of carbon-dioxide clusters by laser-driven Coulomb explosion, Phys. Rev. A **90**, 033411 (2014).

[23] P. Song, X. Wang, C. Meng, W. Dong, Y. Li, Z. Lv, D. Zhang, Z. Zhao, and J. Yuan, Dynamics of three-particle fragmentation of $(CO_2)_2^{3+}$ ions produced by intense femtosecond laser fields, Phys. Rev. A **99**, 053427 (2019).

[24] J. Wu, M. Kunitski, L. P. H. Schmidt, T. Jahnke, and R. Dörner, Structures of N_2Ar, O_2Ar, and O_2Xe dimers studied by coulomb explosion imaging, J. Chem. Phys. **137**, 104308 (2012).

[25] C. A. Schouder, A. S. Chatterley, L. B. Madsen, F. Jensen, and H. Stapelfeldt, Laser-induced Coulomb-explosion imaging of the CS_2 dimer: The effect of non-Coulombic interactions, Phys. Rev. A **102**, 063125 (2020).

[26] X. Yu, Y. Liu, K. Deng, X. Zhang, P. Ma, X. Li, C. Wang, Z. Cui, S. Luo, and D. Ding, Capturing the stereoconfiguration of $(C_6H_6)_2Ar$ by Coulomb-explosion imaging, Phys. Rev. A **105**, 063105 (2022).

[27] A. Khan, T. Jahnke, S. Zeller, F. Trinter, M. Schöffler, L. P. H. Schmidt, R. Dörner, and M. Kunitski, Visualizing the geometry of hydrogen dimers, J. Phys. Chem. Lett. **11**, 2457 (2020).

[28] J. D. Pickering, B. Shepperson, B. A. K. Hübschmann, F. Thorning, and H. Stapelfeldt, Alignment and imaging of the CS_2 dimer inside helium nanodroplets, Phys. Rev. Lett. **120**, 113202 (2018).

[29] J. Zhou, S. Jia, A. D. Skitnevskaya, E. Wang, T. Hähnel, E. K. Grigoricheva, X. Xue, J.-X. Li, A. I. Kuleff, A. Dorn, and X. Ren, Concerted double hydrogen-bond breaking by intermolecular Coulombic decay in the formic acid dimer, J. Phys. Chem. Lett. **13**, 4272 (2022).

[30] J. Zhou, X. Yu, S. Luo, X. Xue, S. Jia, X. Zhang, Y. Zhao, X. Hao, L. He, C. Wang, D. Ding, and X. Ren, Triple ionization and fragmentation of benzene trimers following ultrafast intermolecular Coulombic decay, Nat. Commun. **13**, 5335 (2022).

[31] J. Zhou, S. Jia, X. Xue, A. D. Skitnevskaya, E. Wang, X. Wang, X. Hao, Q. Zeng, A. I. Kuleff, A. Dorn, and X. Ren, Revealing the role of N heteroatoms in noncovalent aromatic interactions by ultrafast intermolecular coulombic decay, J. Phys. Chem. Lett. **15**, 1529 (2024).

[32] L. S. Cederbaum, J. Zobeley, and F. Tarantelli, Giant intermolecular decay and fragmentation of clusters, Phys. Rev. Lett. **79**, 4778 (1997).

[33] G. Öhrwall, M. Tchaplyguine, M. Lundwall, R. Feifel, H. Bergersen, T. Rander, A. Lindblad, J. Schulz, S. Peredkov,

S. Barth, S. Marburger, U. Hergenhahn, S. Svensson, and O. Björneholm, Femtosecond interatomic Coulombic decay in free neon clusters: Large lifetime differences between surface and bulk, Phys. Rev. Lett. **93**, 173401 (2004).

[34] K. Schnorr, A. Senftleben, M. Kurka, A. Rudenko, L. Foucar, G. Schmid, A. Broska, T. Pfeifer, K. Meyer, D. Anielski, R. Boll, D. Rolles, M. Kübel, M. F. Kling, Y. H. Jiang, S. Mondal, T. Tachibana, K. Ueda, T. Marchenko, M. Simon *et al.*, Time-resolved measurement of interatomic Coulombic decay in Ne_2, Phys. Rev. Lett. **111**, 093402 (2013).

[35] J. Ullrich, R. Moshammer, A. Dorn, R. Dörner, L. Ph. H. Schmidt, and H. Schmidt-Böcking, Recoil-ion and electron momentum spectroscopy: Reaction-microscopes, Rep. Prog. Phys. **66**, 1463 (2003).

[36] R. Dörner, V. Mergel, O. Jagutzki, L. Spielberger, J. Ullrich, R. Moshammer, and H. Schmidt-Böcking, Cold target recoil ion momentum spectroscopy: A "momentum microscope" to view atomic collision dynamics, Phys. Rep. **330**, 95 (2000).

[37] S. Jia, J. Zhou, X. Wang, X. Xue, X. Hao, Q. Zeng, Y. Zhao, Z. Xu, A. Dorn, and X. Ren, Cold-target electron-ion-coincidence momentum-spectroscopy study of electron-impact single and double ionization of N_2 and O_2 molecules, Phys. Rev. A **107**, 032819 (2023).

[38] M. J. Frisch, G. W. Trucks, H. B. Schlegel, G. E. Scuseria, M. A. Robb, J. R. Cheeseman, G. Scalmani, V. Barone, G. A. Petersson, H. Nakatsuji, X. Li, M. Caricato, A. V. Marenich, J. Bloino, B. G. Janesko, R. Gomperts, B. Mennucci, H. P. Hratchian, J. V. Ortiz, A. F. Izmaylov *et al.*, Gaussian 16 Revision A.03 (2016), Gaussian, Inc., Wallingford, CT, https://gaussian.com/gaussian16/.

[39] H. B. Schlegel, J. M. Millam, S. S. Iyengar, G. A. Voth, A. D. Daniels, G. E. Scuseria, and M. J. Frisch, *Ab initio* molecular dynamics: Propagating the density matrix with Gaussian orbitals, J. Chem. Phys. **114**, 9758 (2001).

[40] S. S. Iyengar, H. B. Schlegel, J. M. Millam, G. A. Voth, G. E. Scuseria, and M. J. Frisch, *Ab initio* molecular dynamics: Propagating the density matrix with Gaussian orbitals. II. Generalizations based on mass-weighting, idempotency, energy conservation and choice of initial conditions, J. Chem. Phys. **115**, 10291 (2001).

[41] H. B. Schlegel, S. S. Iyengar, X. Li, J. M. Millam, G. A. Voth, G. E. Scuseria, and M. J. Frisch, *Ab initio* molecular dynamics: Propagating the density matrix with Gaussian orbitals. III. Comparison with Born–Oppenheimer dynamics, J. Chem. Phys. **117**, 8694 (2002).

[42] O. Vendrell, S. D. Stoychev, and L. S. Cederbaum, Generation of highly damaging H_2O^+ radicals by inner valence shell ionization of water, ChemPhysChem **11**, 1006 (2010).

[43] J. Zhou, C. He, M.-M. Liu, E. Wang, S. Jia, A. Dorn, X. Ren, and Y. Liu, Real-time observation of ultrafast molecular rotation in weakly bound dimers, Phys. Rev. Res. **3**, 023050 (2021).

[44] A. Bawagan, B. Olsson, K. Tan, J. Chen, and B. Yang, The correlation states of furan and thiophene by high resolution synchrotron photoelectron spectroscopy, Chem. Phys. **164**, 283 (1992).

[45] F. Trinter, J. B. Williams, M. Weller, M. Waitz, M. Pitzer, J. Voigtsberger, C. Schober, G. Kastirke, C. Müller, C. Goihl, P. Burzynski, F. Wiegandt, T. Bauer, R. Wallauer, H. Sann, A. Kalinin, L. P. H. Schmidt, M. Schöffler, N. Sisourat, and T. Jahnke, Evolution of interatomic Coulombic decay in the time domain, Phys. Rev. Lett. **111**, 093401 (2013).

[46] P. Guevara Level, H. Santos Silva, F. Spillebout, K. H. Michaelian, J. M. Shaw, I. Baraille, and D. Bégué, Discerning inter- and intramolecular vibrations of sulfur polyaromatic compounds, J. Phys. Chem. A **121**, 7205 (2017).

[47] X. Ren, E. Jabbour Al Maalouf, A. Dorn, and S. Denifl, Direct evidence of two interatomic relaxation mechanisms in argon dimers ionized by electron impact, Nat. Commun. **7**, 11093 (2016).

[48] X. Ren, E. Wang, A. D. Skitnevskaya, A. B. Trofimov, K. Gokhberg, and A. Dorn, Experimental evidence for ultrafast intermolecular relaxation processes in hydrated biomolecules, Nat. Phys. **14**, 1062 (2018).

[49] P. Możejko, E. Ptasińska-Denga, and C. Szmytkowski, Cross sections for electron collision with five-membered ring heterocycles, Eur. Phys. J. D **66**, 44 (2012).

[50] National institute of standards and technology, mass spectrum (electron ionization) of thiophene, in *NIST Chemistry WebBook*, NIST Standard Reference Database 69 (U.S. Department of Commerce, Washington, DC, 1998).

[51] E. Rennie, D. Holland, D. Shaw, C. Johnson, and J. Parker, A study of the valence shell spectroscopic and thermodynamic properties of thiophene by photoabsorption and photoion spectroscopy, Chem. Phys. **306**, 295 (2004).

[52] J. Zhou, M. Belina, S. Jia, X. Xue, X. Hao, X. Ren, and P. Slavíček, Ultrafast charge and proton transfer in doubly ionized ammonia dimers, J. Phys. Chem. Lett. **13**, 10603 (2022).

[53] S. Zeller, M. Kunitski, J. Voigtsberger, M. Waitz, F. Trinter, S. Eckart, A. Kalinin, A. Czasch, L. P. H. Schmidt, T. Weber, M. Schöffler, T. Jahnke, and R. Dörner, Determination of interatomic potentials of He_2, Ne_2, Ar_2, and H_2 by wave function imaging, Phys. Rev. Lett. **121**, 083002 (2018).

[54] X. Yu, X. Hu, J. Zhou, X. Zhang, X. Zhao, S. Jia, X. Xue, D. Ren, X. Li, Y. Wu, X. Ren, S. Luo, and D. Ding, Measuring charge distribution of molecular cations by an atomic Coulomb probe microscope, Chin. Phys. Lett. **39**, 113301 (2022).